BOUNDARY INTEGRAL METHODS APPLIED TO
CAVITATION BUBBLE DYNAMICS

Bachok Taib, G. Doherty and J.R. Blake

1. INTRODUCTION

Cavitation can occur in fast moving liquids whenever the local pressure in the liquid falls below a certain critical value (the vapour pressure) for a sufficient time. Bubbles form in a low pressure region and are swept away to regions of higher pressure where they collapse creating extremely high local velocities and pressure immediately adjacent to the bubble. This leads to noise, vibration and physical damage if the collapse occurs close to a solid boundary. Cavitation is a problem that has continuously plagued engineers in a variety of disciplines ranging from the aerospace engineer designing rocket pumps to the civil engineer concerned with the service life of spillway structures and energy dissipators. Cavitation can occur in fluid machinery: in all types of centrifugal pumps, also in turbines, propellers, underwater missiles, torpedoes and in piping systems near elbows, contractions and expansions of the pipe (see Arndt [1] for expansion on the above discussion).

The main objectives of our research programme in Cavitation Bubble Dynamics is to gain a better understanding of the potential mechanisms for causing damage to turbomachinery and other hydraulic devices (e.g. pitting, erosion). It is now thought that the damage mechanism is primarily due to a very high speed liquid jet impacting against the boundary. However, the direction and speed of the jet depends on the properties of the boundary; for example a rigid boundary "attracts"

bubbles with the jet directed towards the boundary, whereas a free surface "repels" bubbles with the jet directed away from the boundary, (see e.g. Benjamin and Ellis [2], Plesset and Chapman [12], Blake and Gibson [5], Gibson and Blake [7]). The major objective of our study is to determine the parameter space of the physical properties of compliant boundaries which will just repel collapsing cavitation bubbles.

In this paper we plan to illustrate one aspect of this study; notably the application of boundary integral methods to the growth and collapse of a cavitation bubble near a rigid boundary. We calculate the shape of the bubble, pressure contours and particle paths as a function of the bubble lifetime. Other aspects of the experimental and theoretical research programme may be found in other publications of the group (see e.g. Blake and Gibson [5], Gibson and Blake [7,8], Blake and Cerone [4], Blake [3]).

To simulate the growth and collapse of a cavitation bubble near a rigid boundary the fluid mechanics will be modelled by an incompressible, inviscid and irrotational fluid flow. This yields Laplace's equation for the velocity potential, thus enabling us to apply the boundary integral method using the moving surface of the cavitation bubble. In the next section we develop techniques for solving the boundary integral equations for a bubble in an infinite fluid. These ideas are extended in the succeeding section to that of a cavitation bubble near a rigid boundary, in particular concentrating on the solution strategy where the nonlinearities are incorporated into the updating of the boundary conditions. A discussion of the physical significance and implications of our calculations may be found in the final section.

However before moving to the development of our solution technique incorporating the boundary method we present the classic solution of Lord Rayleigh [13] for a cavitation bubble in an infinite fluid. This is particularly important when checking and comparing results from our numerical procedure. Briefly if linear dimensions are scaled with respect to the maximum bubble radius R_m and time scale of $R_m/[(p_\infty - p_C)/\rho]^{\frac{1}{2}}$ (p_∞, pressure at infinity; p_C, vapour pressure; ρ, density) are introduced, then the velocity and pressure field are given by

$$
(1) \quad
\begin{cases}
v(r,t) = \dfrac{R^2 \dot{R}}{r^2} \\[4mm]
p(r) = 1 + \dfrac{1}{r}\left[\dfrac{1-4R^3}{3R^2}\right] - \dfrac{1}{r^4}\left[\dfrac{1}{3} R(1-R^3)\right]
\end{cases}
$$

where $R(t)$ $(0 \le R \le 1)$ is the bubble radius and r is the radius in spherical polar coordinates. The lifetime of a Rayleigh bubble is $T = 1.829$. The maximum pressure is given by

$$
(2) \quad p_{max} =
\begin{cases}
p(r_1) : r_1 = \left[\dfrac{4(R^3 - R^6)}{1 - 4R^3}\right]^{\frac{1}{3}} & R \le 0.6299 \\[4mm]
1 : \text{at } \infty \, ; & R > 0.6299 \, .
\end{cases}
$$

As an illustration, when $R = 0.1$, the maximum pressure $p_{max} = 157.7030$ occurs at $r_1 = 0.1589$. Thus for example, if $p_\infty - p_C$ was 1 atmosphere, the maximum pressure would be 157 atmospheres just outside the collapsing bubble.

For non-spherically symmetric bubbles an alternative technique is required: one approach will be described in the next section using a boundary integral method.

2. BOUNDARY INTEGRAL METHOD

2.1 Formulation.

For any sufficiently smooth function ϕ which satisfies Laplace's equation with a domain Ω having piecewise smooth surface S, Green's integral formula can be written (Jaswon and Symm [11])

$$(3) \qquad c(p)\,\phi(p) \; + \int_S \phi(q)\,\frac{\partial}{\partial n}\!\left(\frac{1}{|p-q|}\right) dS \; = \int_S \frac{\partial}{\partial n}\,\phi(q)\,\frac{1}{|p-q|}\,dS$$

where $p \in \Omega + S$, $q \in S$, $\dfrac{\partial}{\partial n}$ is the normal derivative outward from S, and

$$(4) \qquad c(p) \; = \; \begin{cases} 4\pi & \text{if} \quad p \in \Omega \\ 2\pi & \text{if} \quad p \in S. \end{cases}$$

Choosing p on S yields an equation for either ϕ or $\dfrac{\partial\phi}{\partial n}$ on S if the other is specified. Once both are known on S, equation (3) can be used to generate ϕ at any interior point p. In axisymmetric problems, ϕ and $\dfrac{\partial\phi}{\partial n}$ are independent of rotational angle and integration over this variable can be performed analytically.

2.2 Axisymmetric form of the integrals.

Using cylindrical polar coordinates with $p = (r_0, 0, z_0)$ and $q = (r, \theta, z)$ respectively,

$$(5) \qquad \left| \frac{1}{p-q} \right| = \frac{1}{[(r+r_0)^2 + (z-z_0)^2 - 4rr_0\cos^2\theta/2]^{\frac{1}{2}}}\;.$$

If the surface S is parametrized by the arc length variable ξ

$$(6) \qquad \int_S dS\,\frac{1}{|p-q|} = \int_0^1 d\xi\,\frac{4r(\xi)\left[\left(\frac{dz}{d\xi}\right)^2 + \left(\frac{dr}{d\xi}\right)^2\right]^{\frac{1}{2}}}{\left[\left(r(\xi)+r_0\right)^2 + \left(z(\xi)-z_0\right)^2\right]^{\frac{1}{2}}}\,K(k)$$

and

$$(7) \qquad \int_S dS \, \frac{\partial}{\partial n} \frac{1}{|p-q|} \; = \; \int_0^1 d\xi \, \frac{4r(\xi)}{[\left(r(\xi)+r_0\right)^2 + \left(z(\xi)-z_0\right)^2]^{3/2}}$$

$$\times \left\{ \left[\frac{dz}{d\xi}\left(r(\xi)+r_0\right) - \frac{dr}{d\xi}\left(z(\xi)-z_0\right) - \frac{2}{k^2(\xi)} \frac{dz}{d\xi} r_0 \right] \frac{E(k)}{1-k^2(\xi)} + \frac{2}{k^2(\xi)} \frac{dz}{d\xi} r_0 K(k) \right\}$$

where

$$(8) \qquad k^2(\xi) \; = \; \frac{4r(\xi)r_0}{\left(r(\xi)+r_0\right)^2 + \left(z(\xi)-z_0\right)^2}$$

and $K(k)$, $E(k)$ are the complete elliptic integrals of the first and
second kind. Approximations for these functions are available in Hastings
[10] in the form

$$(9) \qquad \begin{aligned} K(k) &= P(x) - Q(x) \, \ln x, \\ E(k) &= R(x) - S(x) \, \ln x, \end{aligned}$$

where

$$(10) \qquad x = 1 - k^2(\xi),$$

and

P, Q, R, and S are tabulated polynomials.

2.3 Surface approximation.

To proceed with the computation, we need to choose a representation
for the surface of the bubble, and also for the potential and its normal
derivative on the surface. To some extent, these choices can be
independent, but as the movement of the surface is computed using the
potential and its derivative, the two should be considered together. In
the description which follows, a plane section through the axis of symmetry
of the bubble is taken, and rotational symmetry about the axis is understood.

2.4 Linear surface - constant functions.

The surface is replaced by a set of N linear segments S_j, with the potential and its normal derivative constant on each segment. The boundary integral equation is replaced by its collocation form using the midpoint of each linear segment.

$$(11) \qquad 2\pi\phi_i + \sum_{j=1}^{N} \phi_j \int_{S_j} \frac{\partial}{\partial n} \left| \frac{1}{p_i - q_j} \right| dS = \sum_{j=1}^{N} \frac{\partial}{\partial n} (\phi_j) \int_{S_j} \frac{1}{|p_i - q_j|} dS .$$

If we denote $\frac{\partial \phi}{\partial n}$ by ψ, we can write (11) in matrix form (as for example in Brebbia [6]) as

$$(12) \qquad 2\pi\phi_i + \sum_{j=1}^{N} \hat{H}_{ij} \phi_j = \sum_{j=1}^{N} G_{ij} \psi_j .$$

Defining $H_{ij} = \hat{H}_{ij} + 2\pi \delta_{ij}$ (12) may be written as

$$(13) \qquad H\phi = G\psi .$$

2.5 Linear surface - linear functions.

ϕ_j and ψ_j are assumed to be single valued at the end points of the linear segments which approximate the surface. If the segment is parametrized by ξ in the range $(0,1)$ we can define

$$(14) \qquad \begin{aligned} M_1(\xi) &= 1 - \xi \\ M_2(\xi) &= \xi \end{aligned}$$

and use the isoparametric approximations for both the surface and the functions. On segment S_j we have,

$$(15) \qquad \begin{aligned} r(\xi) &= r_{j-1}M_1(\xi) + r_j M_2(\xi) \\ z(\xi) &= z_{j-1}M_1(\xi) + z_j M_2(\xi) \\ \phi(\xi) &= \phi_{j-1}M_1(\xi) + \phi_j M_2(\xi) \\ \psi(\xi) &= \psi_{j-1}M_1(\xi) + \psi_j M_2(\xi) . \end{aligned}$$

The collocation points are moved to the end points of the interval, yielding N+1 equations in the N+1 unknowns. The integrals on each segment can be written

(16)
$$\int_{S_j} dS \, \frac{\partial \phi}{\partial n} \, \frac{1}{|p_i - q_j|} = b_{1ij} \psi_{j-1} + b_{2ij} \psi_j$$

where

(17)
$$b_{kij} = S_j \int_0^1 d\xi M_k(\xi) \int_0^{2\pi} d\theta \, \frac{1}{|p_i - q(\xi, \theta)|}$$

(18)
$$\int_{S_j} dS \, \phi \, \frac{\partial}{\partial n} \, \frac{1}{|p_i - q_j|} = a_{1ij} \phi_{j-1} + a_{2ij} \phi_j$$

where

(19)
$$a_{kij} = S_j \int_0^1 d\xi M_k(\xi) \int_0^{2\pi} d\theta \, \frac{\partial}{\partial n} \, \frac{1}{|p_i - q(\xi, \theta)|} \, .$$

2.6 Numerical integration.

The evaluation of the elements of the matrices H and G is performed numerically. Normally Gauss Legendre quadrature is adequate, unless the collocation point p_i is within the segment S_j, or is one of its endpoints, in which case the integrand is singular and must be treated specially. The singular integrals are evaluated by subtracting a logarithm term to remove the singularity, then using a quadrature scheme incorporating the logarithm to complete the integration.

As an example, consider the case where p_i is at the midpoint ($\xi = \frac{1}{2}$) of the interval S_j. A typical integral would be

(20)
$$\int_S \frac{dS}{|p - q|} = \int_0^1 d\xi \, \frac{4 r(\xi) \left[\left(\frac{dz}{d\xi}\right)^2 + \left(\frac{dr}{d\xi}\right)^2 \right]^{\frac{1}{2}} K(k)}{\left[\left(r(\xi) + r_0\right)^2 + \left(z(\xi) - z_0\right)^2 \right]^{\frac{1}{2}}}$$

where p is the point $(r_0, z_0) = \left(r(\frac{1}{2}), z(\frac{1}{2})\right)$.

Recalling

(21)
$$k^2(\xi) = \frac{4r(\xi)\,r_0}{\left(r(\xi)+r_0\right)^2 + \left(z(\xi)-z_0\right)^2}$$

(22)
$$x = 1 - k^2(\xi) = \frac{\left(r(\xi)-r_0\right)^2 + \left(z(\xi)-z_0\right)^2}{\left(r(\xi)+r_0\right)^2 + \left(z(\xi)-z_0\right)^2}$$

then around $\xi = \tfrac{1}{2}$,

(23)
$$x = 1 - k^2(\xi) \approx \frac{(\xi-\tfrac{1}{2})^2}{4r_0^2}\left[\left(\frac{dr}{d\xi}\right)^2 + \left(\frac{dz}{d\xi}\right)^2\right] ,$$

so that the elliptic integral $K(k)$ behaves like

$$K(k) \approx P(x) - Q(x)\,\ell n[A(\xi-\tfrac{1}{2})^2] .$$

This allows the integral of equation (20) to be replaced by

(25)
$$\int_0^1 d\xi\; \frac{4r(\xi)\left[\left(\frac{dz}{d\xi}\right)^2 + \left(\frac{dr}{d\xi}\right)^2\right]^{\frac{1}{2}}}{[\left(r(\xi)+r_0\right)^2 + \left(z(\xi)-z_0\right)^2]^{\frac{1}{2}}}\; [K(k) + 2Q(x)\,\ell n(|\xi-\tfrac{1}{2}|)]$$

$$+ 2\int_0^1 d\xi\; \ell n\!\left(\frac{1}{|\xi-\tfrac{1}{2}|}\right) Q(x)\; \frac{4r(\xi)\left[\left(\frac{dz}{d\xi}\right)^2 + \left(\frac{dr}{d\xi}\right)^2\right]^{\frac{1}{2}}}{[\left(r(\xi)+r_0\right)^2 + \left(z(\xi)-z_0\right)^2]^{\frac{1}{2}}} .$$

The first integral contains no singularity, and can be integrated by standard Gauss Legendre quadrature. The second integral contains an explicit singularity of log type which can be integrated using the quadrature scheme tabulated by Stroud and Secrest [14] for the integral

$$\int_0^1 dx\; \ell n\!\left(\frac{1}{x}\right) f(x) .$$

Similar techniques can be used to remove the singularities from the other singular integrals.

An additional device which has proved helpful in increasing the numerical accuracy of the computation has been to replace the diagonal

elements of the matrix H by

(26)
$$H_{ii} = 4\pi - \sum_{j \neq i} H_{ij} \ .$$

This property may be deduced from the fact that for the interior problem,
the matrix equation

$$H\phi = G\psi$$

with ϕ constant at all points on the boundary (the Dirichlet problem)
should yield $\psi \left(= \dfrac{\partial \phi}{\partial n} \right)$ zero at all points, while ψ specified at all
points on the boundary (the Neumann problem) yields a solution for
which contains an arbitrary additive constant. Thus, for the interior
problem,

(27)
$$H_{ii} = - \sum_{j \neq i} H_{ij} \ ,$$

and consideration of the definition of H leads immediately to equation
(26) for the exterior problem.

3. EQUATIONS OF MOTION

Assuming the fluid to be incompressible and inviscid, and ignoring
surface tension and gravitational effects (Plesset and Chapman [12],
Blake and Gibson [5], and Guerri, Lucca and Prosperetti [9]), the velocity
in the fluid may be written

(28)
$$\underline{u} = \nabla \phi$$

where ϕ satisfies Laplace's equation

(29)
$$\nabla^2 \phi = 0 \ .$$

On the bubble surface the pressure p is given by

(30)
$$p = p_c$$

where p_c is the saturated vapour pressure in the bubble. As fluid

particles remain on the surface of the bubble we may simply equate the

velocity of the bubble surface $\underline{u}_S$ to the fluid particle velocity

(31) $\underline{u}_S(\underline{r}) = \underline{u}(\underline{r}), \quad \underline{r} \in S$.

The boundary conditions at infinity are

(32)
$$\underline{u} \to 0$$
$$p \to p_\infty$$

In the case of a bubble growing adjacent to a rigid boundary at $z = 0$,

no flow through the boundary requires

(33) $\dfrac{\partial \phi}{\partial z} = 0$ at $z = 0$.

   In terms of the potential, equation (31) for the movement of the

boundary $\underline{r}$ becomes

(34) $\dfrac{d\underline{r}}{dt} = \nabla \phi$.

By using the Bernoulli equation on the bubble surface,

(35) $p_c = p_\infty - \rho \dfrac{\partial \phi}{\partial t} - \tfrac{1}{2} \rho |\underline{u}|^2$,

we are able to obtain an expression for the rate of change of potential

on the bubble surface as follows,

(36) $\dfrac{D\phi}{Dt} = \dfrac{\partial \phi}{\partial t} + \nabla \phi \cdot \dfrac{d\underline{r}}{dt} = \dfrac{p_\infty - p_c}{\rho} + \dfrac{1}{2} |\underline{u}|^2$.

Equations (34) and (36) will be used during the computation to update both

the shape of the bubble and the potential on its surface.

   Finally to specify a well-posed problem we require some initial

conditions. To do this we suppose the growth of the bubble is started from

a very small spherical bubble of radius R_0 with the potential obtained

from the Rayleigh bubble solution in an infinite fluid (Blake and Gibson

[5]).

$$(37) \qquad \phi_0 = -R_0 \left[\frac{2}{3} \left(\frac{P_\infty - P_c}{\rho} \right) \left\{ \left(\frac{R_m}{R_0} \right)^3 - 1 \right\} \right]^{\frac{1}{2}}$$

where R_m is the maximum bubble radius. In the next section we proceed to obtain a numerical solution of the above equations.

4. COMPUTATIONAL RESULTS

4.1 Solution strategy.

The strategy of solution is as follows: since initially we know the position of the bubble surface and the potential ϕ on the surface we can solve the discretized form of the boundary integral equation (13) to yield the value of the normal velocity $\frac{\partial \phi}{\partial n}$ on the bubble surface. With the prior knowledge of ϕ on S we can calculate the tangential velocity $\frac{\partial \phi}{\partial S}$ and hence, together with $\frac{\partial \phi}{\partial n}$, $\nabla \phi$, the particle velocity on S. Immediately we can update the bubble shape by using a simple Euler scheme as follows

$$(38) \qquad \underline{r}(t+\Delta t) = \underline{r}(t) + \Delta t \, \nabla \phi + O(\Delta t^2)$$

and as well by exploiting (36), the updated surface potential

$$(39) \qquad \phi \big(r(t+\Delta t), t+\Delta t \big) = \phi \big(r(t), t \big) + \Delta t \, \frac{D\phi}{Dt} + O(\Delta t^2)$$

with a time step chosen to limit the change in the potential ϕ. This procedure is repeated throughout the growth and collapse phases of the bubble until just prior to the bubble becoming multiply connected. Experiments with more elaborate time integration techniques will be reported in Taib [15].

4.2 Rayleigh bubble.

The first problem studied is the Rayleigh bubble, a single spherical bubble growing and collapsing in an infinite fluid. Instability started

to occur in our calculation for a dimensionless bubble radius of 1.5142×10^{-2} at dimensionless time $T = 1.825$, in reasonable agreement with the exact lifetime of 1.829. These results were obtained with the bubble surface divided into 16 linear segments, with a linear approximation of the potential and its derivative on each segment.

4.3 Rigid boundary.

The second problem, for which more detailed results are presented, is the growth and collapse of a cavitation bubble near to a rigid boundary. The condition of no flow through the boundary is incorporated into the calculation by the use of an image bubble in the computation of potential and its normal derivative. In these calculations 28 linear segments were used to represent the boundary with closer spacing near to the axis of symmetry.

4.4 Dimensionless variables.

The reduction to dimensionless variables is made with respect to the maximum bubble radius R_m.

$$(40) \qquad Z = \frac{z}{R_m}, \quad R = \frac{r}{R_m}, \quad \gamma = \frac{h}{R_m}$$

where h is the initial distance between the bubble centroid and the rigid boundary. The other variables are made dimensionless by the following transformations

$$(41) \qquad T = \frac{t}{R_m}\left(\frac{p_\infty - p_c}{\rho}\right)^{\frac{1}{2}}$$

$$(42) \qquad P = \frac{p - p_c}{p_\infty - p_c}$$

$$(43) \qquad \Phi = \frac{\phi}{R_m}\left(\frac{\rho}{p_\infty - p_c}\right)^{\frac{1}{2}}$$

Calculations are reported in terms of the above dimensionless quantities.

5. BUBBLE SHAPE, PARTICLE PATHS AND PRESSURE CONTOURS

With the strategy of solution outlined in the previous section we are able to calculate and plot the bubble shape, particle paths and pressure contours as functions of time for different values of γ, the initial location of the bubble centroid relative to the rigid boundary. In this paper we have chosen two values of γ for discussion; namely $\gamma = 1.0$ and 1.5. Gibson (see e.g. Gibson and Blake [7]) has conducted a series of experiments over a range of values of γ and we find that our theoretically predicted bubble shapes compare very favourably with his experiments.

5.1   Bubble shape.

The bubble shapes at selected dimensionless times T are shown in figures 1 and 2 for $\gamma = 1.5$ and 1.0 respectively. It can be seen that the lifetime of the bubble is extended when the growth begins nearer to the boundary (i.e. smaller values of γ).

For the case $\gamma = 1.5$, the bubble shapes we obtained are in general agreement with those obtained by Plesset and Chapman [12], and those obtained by Guerri, Lucca and Prosperetti [9]. However in our model the collapse occurred much nearer to the rigid boundary, indicating the importance of explicitly considering the growth phase.

For $\gamma = 1.0$, Plesset and Chapman [12] obtained bubble shapes which are more elongated than those we obtained here, again indicating the importance of the growth phase. We have separately modelled the case $\gamma = 0.96$ where we obtain very good agreement with the experimental results reported in Gibson and Blake [7], hence confirming our views on the importance of the growth phase.
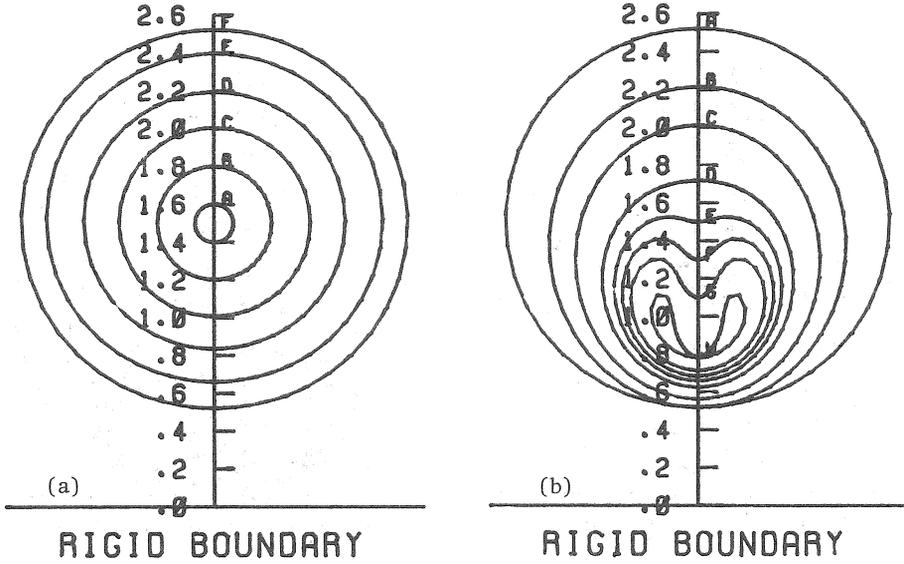
Figure 1.   Bubble shapes for γ = 1.5 during (a) expansion phase at
dimensionless times A) 0.001553 B) 0.024138 C) 0.090953 D) 0.214281
E) 0.466561 F) 0.973926 and (b) collapse phase at dimensionless times
A) 0.973926 B) 1.729799 C) 1.881328 D) 1.988787 E) 2.024132
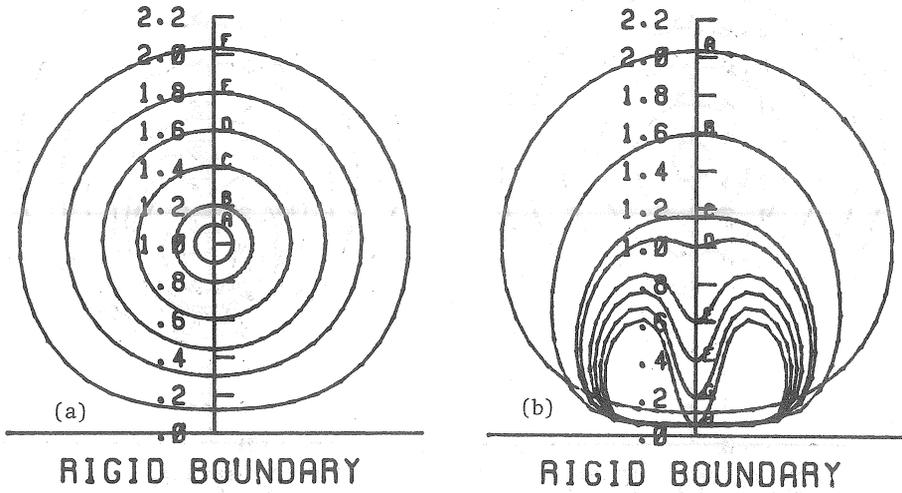F) 2.044900 G) 2.063839 H) 2.093078.

Figure 2. Bubble shapes for $\gamma = 1.0$ during (a) expansion phase at dimensionless times A) 0.001553 B) 0.009084 C) 0.053140 D) 0.142416 E) 0.312960 F) 0.975561 and (b) collapse phase at dimensionless times A) 0.975561 B) 1.849750 C) 2.023160 D) 2.048726 E) 2.097308 F) 2.121807 G) 2.144854 H) 2.162422.

5.2   Particle paths.

Figure 3 shows the pathlines of selected particles on the bubble surface, together with three shapes of bubble, the initial, the maximum and the final. We notice that the particles move radially during the growth phase, however during the collapse phase, the particles migrate towards the axis of symmetry except when in the liquid jet where they move almost parallel to the axis of symmetry.

5.3   Pressure contours.

Pressure at any point in the fluid can be calculated using the Bernoulli condition

$$p = p_\infty - \rho \, \frac{\partial \phi}{\partial t} - \tfrac{1}{2} \, \rho \, |\underline{u}|^2 \ .$$

In our calculation we use the following difference approximation of $\frac{\partial \phi}{\partial t}$

(44) $$\frac{\partial \phi}{\partial t} \approx \frac{(\Delta t_{n-1})^2 \phi_{n+1} - [(\Delta t_{n-1})^2 - (\Delta t_n)^2] \phi_n - (\Delta t_n)^2 \phi_{n-1}}{\Delta t_n \Delta t_{n-1} (\Delta t_n + \Delta t_{n-1})}$$

where $\Delta t_n = t_{n+1} - t_n$. With our prior knowledge of $\underline{u}$ we can now calculate the dynamic pressure p anywhere in the fluid.

In figure 4 we illustrate the pressure contours at several times late in the collapse phase for the $\gamma = 1.0$ example. From the Rayleigh bubble solution we might anticipate a maximum pressure occurring close to the bubble surface and, because of the loss of spherical symmetry in the rigid boundary example, the point of maximum pressure occurs on the axis of symmetry. A physical explanation of the above phenomena is as follows. At the start of the collapse phase the maximum pressure occurs at infinity (equal to 1 in our dimensionless terms) causing the fluid to accelerate towards the bubble (i.e. the bubble is acting as a sink). However as the collapse continues mass conservation demands that the bulk of the fluid some distance away from the bubble must decelerate (we do not have a black hole!) creating a point of maximum pressure close to the collapsing bubble
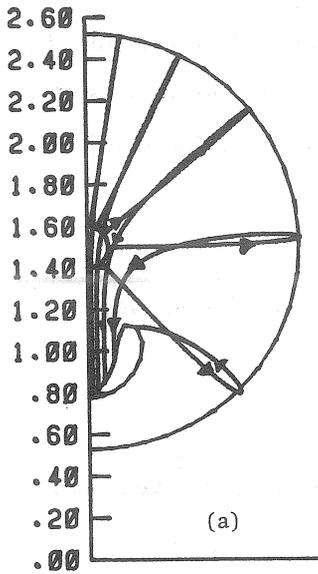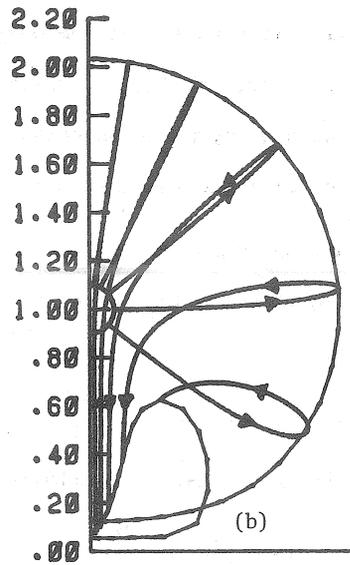
Figure 3. Pathlines of selected fluid particles on the bubble surface for the case a) γ = 1.5 and b) γ = 1.0. The bubbles shown are the initial, maximum and the final shape respectively.
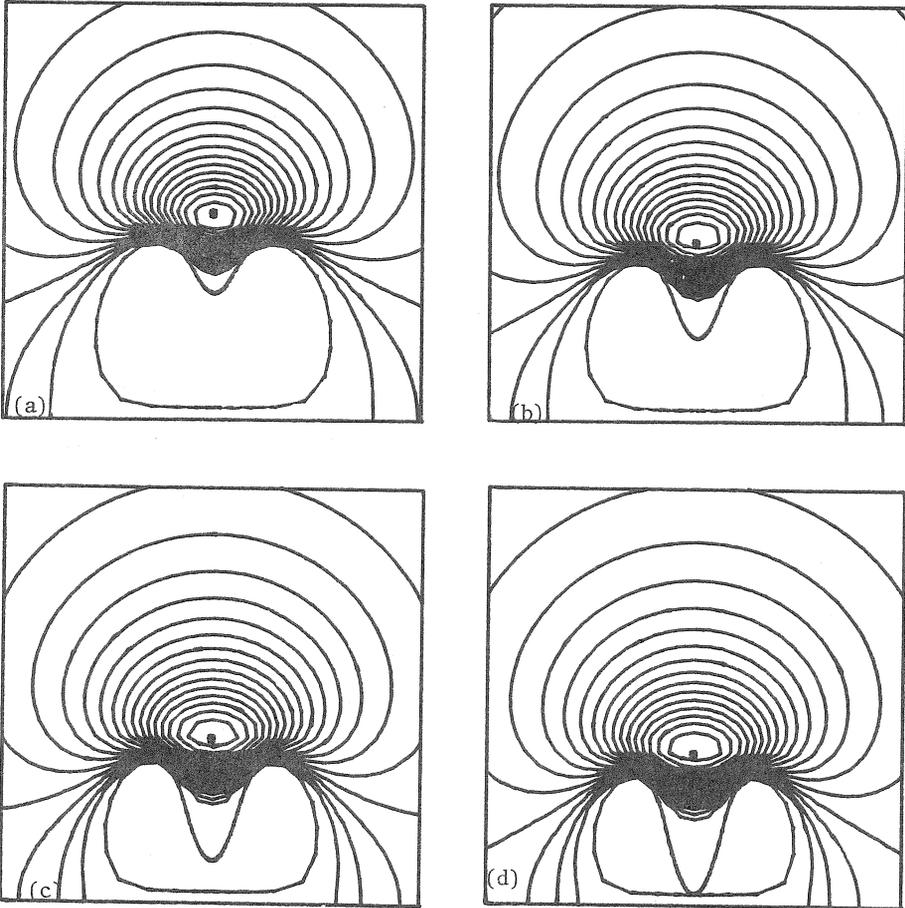
Figure 4.   Pressure contours for $\gamma = 1$ at time a) 2.09308
b) 2.121807 c) 2.1448544 and d) 2.162422. Maximum pressure at
* of a) 7.2269 b) 7.6117 c) 8.0510 and d) 8.4018.

surface. In other words the acceleration of the fluid is zero at this point (i.e. $\nabla p = 0$). Conversely the small volume of fluid between the point of maximum pressure and the bubble is being continually accelerated creating the very high speed liquid jet so clearly evident in figures 1, 2 and 3.

6. CONCLUSIONS

This paper has been primarily concerned with the development of a boundary integral method to model the growth and collapse of a cavitation bubble near a rigid boundary. The method allows us to calculate in fine detail, and to high accuracy, the relevant physical quantities such as jet speed, pressure field and particle trajectories. These calculations together with further work to be reported in Taib [15] will lead to a much enhanced understanding of the physical mechanisms responsible for cavitation damage.

7. ACKNOWLEDGEMENTS

REFERENCES

[1]   R.E.A. Arndt, "Recent advances in cavitation research", *Advances in Hydroscience* 12 (1981), 1-78.

[2]   T.B. Benjamin and A.T. Ellis, "The collapse of cavitation bubbles and the pressure thereby produced against solid boundaries", *Trans. Roy. Soc.* A260 (1966), 221-240.

[3]   J.R. Blake, "The Kelvin impulse: application to bubble dynamics", *Proc. 8th Aust. Fluid Mech. Conf.*, Newcastle 2 (1983), 10B.1-10B.4.

[4]   J.R. Blake and P. Cerone, "A note on the impulse due to a vapour bubble near a boundary", *J. Aust. Math. Soc.* B23 (1982), 383-393.

[5]   J.R. Blake and D.C. Gibson, "Growth and collapse of a vapour cavity near a free surface", *J. Fluid Mech.* 111 (1981), 123-140.

[6]   C.A. Brebbia, *The Boundary Element Method for Engineers*, Pentech Press, London, 1978.

[7]   D.C. Gibson and J.R. Blake, "Growth and collapse of cavitation bubbles near flexible boundaries", *Proc. 7th Aust. Hydraulics and Fluid Mech. Conf.*, Brisbane (1980) 283-286.

[8]   D.C. Gibson and J.R. Blake, "The growth and collapse of bubbles near deformable surfaces", *Appl. Sci. Res.* 38 (1982), 215-224.

[9]   L. Guerri, G. Lucca and A. Prosperetti, "A numerical method for the dynamics of non-spherical cavitation bubbles", *Proc. 2nd Int. Colloq. on drops and bubbles*, California (1981), 175-181.

[10]   C. Hastings Jr., *Approximations for digital computers*, Princeton University Press, Princeton, N.J., 1955.

[11]   M.A. Jaswon and G.I. Symm, *Integral equation methods in potential theory and elastostatics*, Academic Press, London, 1977.

[12]   M.S. Plesset and R.B. Chapman, "Collapse of an initially spherical vapour cavity in the neighbourhood of a solid boundary", *J. Fluid Mech.* <u>47</u> (1971), 283-290.

[13]   Lord Rayleigh, "On the pressure developed in a liquid during the collapse of a spherical void", *Phil. Mag.* <u>34</u> (1917), 94-98.

[14]   A.H. Stroud and D. Secrest, *Gaussian quadrature formulas*, Prentice-Hall, Englewood Cliffs, N.Y., 1966.

[15]   B.B. Taib, *Boundary integral equation method in hydrodynamics*, Ph.D. Thesis, Department of Mathematics, The University of Wollongong, N.S.W., Australia, 1984.

Department of Mathematics,
University of Wollongong,
P.O. Box 1144,
Wollongong,
New South Wales 2500
AUSTRALIA.